Modeling the Morphology Development of Ethylene Copolymers in Rotational Molding

H. Xu, C. T. Bellehumeur

Department of Chemical and Petroleum Engineering, Schulich School of Engineering, University of Calgary, Calgary, AB, Canada T2N 1N4

Received 3 March 2006; accepted 12 June 2006
DOI 10.1002/app.25092
Published online in Wiley InterScience (www.interscience.wiley.com).

ABSTRACT: A model is proposed to describe the solidification and crystallization phenomena in rotational molding. To capture the morphology development with crystallization behavior, a two-dimensional theoretical simulation was carried out, consisting of a phase-field model emphasizing the metastability of polymer crystallization and a heat-transfer model describing the molding cycle. The model parameters were experimentally evaluated with differential scanning calorimetry and isothermal crystallization tests. Molding trials were also conducted with bench-scale rotational molding equipment, and the cross sections of the molded products were examined under polarized light optical microscopy. The model predictions capture the formation of transcrystalline structures near the mold surface, which is more apparent under moderate cooling conditions. Our results show that the model predictions are in general agreement with the experimental results obtained in our laboratory as well as those presented in the literature. Because morphological features are important contributing factors to product performance, the model will be useful for the formulation of new materials and process optimization. © 2006 Wiley Periodicals, Inc. J Appl Polym Sci 102: 5903–5917, 2006

Key words: crystallization; modeling; molding; morphology; polyolefins

INTRODUCTION

The rotational-molding process is used to fabricate hollow, plastic products, as illustrated in Figure 1. Many thermoplastics used in rotational-molding applications are semicrystalline in nature, with polyethylenes accounting for over 80% of the production. Unlike most other processes, rotational molding does not use pressure to force the melt into a shape but relies primarily on the gradual deposition and adhesion of the polymer onto the mold. The heating and cooling of the mold rely mostly on the convective transport of energy. The most common method of heating is gas combustion, whereas cooling relies on exposing the mold to forced air flow, water mist, water spray, or a combination of these methods. A large amount of effort has been spent on modeling and optimizing the process and on developing new resins and new applications for rotational molding. Effort has been devoted to the problem of powder densification in recent years[1,2] since it greatly influences the quality of the molded product and often dictates the choice of processing conditions during the heating cycle. The solidification stage is also of great importance. The final morphology greatly contributes to the performance of the end product, which can be defined on the basis of the stiffness, dimensional stability, barrier properties, chemical resistance, and impact properties according to the final application of the molded part. However, only a few studies have been devoted to this topic.[3–5] The consideration of microstructures that are formed on different scales is often required to describe the physical and mechanical properties of molded parts. They can be divided into the following categories: (1) a macroscopic scale, which captures the advancing solidification front, and consists of spherulitic domains mixed with the melt; (2) a mesoscopic scale, at which individual spherulites can be examined; (3) a nanoscopic scale, which captures the lamellar structure composing the spherulites; and (4) a molecular scale, which is concerned with interactions occurring between chain segments. Although the property dependence of semicrystalline polymers on their microstructure is widely accepted, the establishment of useful relationships is not always straightforward for several structural parameters can be affected by changes in the material properties (molecular structure and chemical composition) and processing conditions.

In most polymer processes, crystallization normally takes place at temperatures below the melting temperature (T_m) and usually under highly nonisother-

Correspondence to: C. T. Bellehumeur (cbellehu@ucalgary.ca).

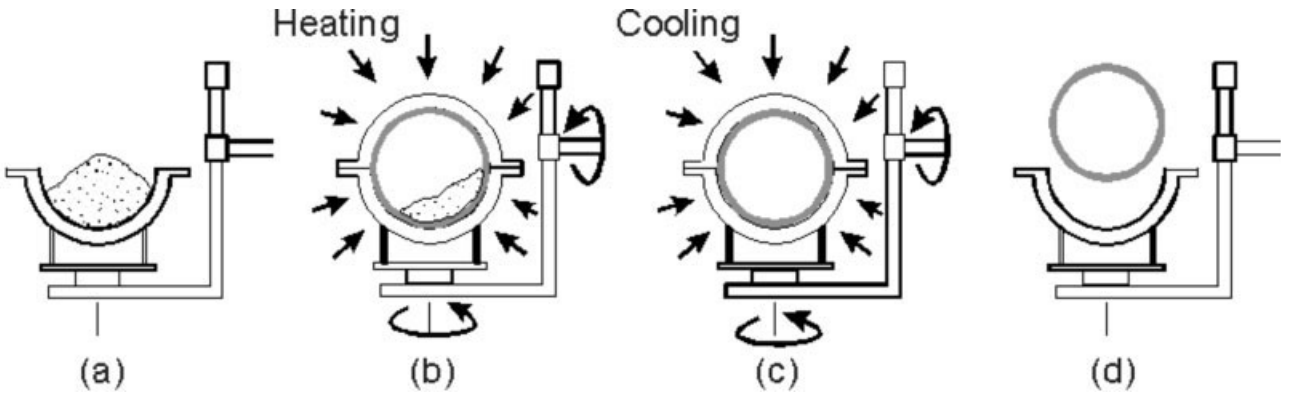

Figure 1 (a) The polymer is first loaded into a mold, usually in a powder form. (b) The mold and its content are heated and rotated about its two primary axes, and the tumbling powder gradually melts, sticks to the mold surface, and densifies. (c) The mold and its content are cooled. (d) The molded part is removed once it has reached a temperature safe for manual handling.

mal conditions. The rate of crystallization is known to be a strong function of temperature and can also be accelerated by orders of magnitude when polymer melts are simultaneously subjected to flow deformation. An important aspect of rotational molding is that the heating and cooling rates cover a wide range, yet they are very low compared with those of other processes. Moreover, rotational molding is distinct from other processes as the melting and solidification occur in a nearly shear-free environment. As a result, large spherulites and other crystallization morphologies appear in the parts. Only one surface (the outer surface) of the plastic product is in contact with the metal mold; the other free surface (the inner surface) is exposed to air and is more susceptible to thermooxidative degradation. Semicrystalline polymers in rotational molding undergo asymmetrical cooling, which creates a crystallization front moving from the outer surface toward the inner wall. Variations in the morphological features, which were first reported by Cramez et al.,[3] have been attributed mainly to the inherent differences in the thermal history imposed on the material across the thickness of the molded part.

Solidification and crystallization phenomena during rotational molding are greatly affected by the presence of endothermic and exothermic transitions, which determine the temperature gradient along the thickness of the part. Theoretical heat transfer models for the entire rotational molding process have been proposed and used to predict the internal air temperature profile as well as the temperature distribution inside the molded part.[6–10] Given the predicted temperature distribution with the heat transfer model, it is possible to simulate two-dimensional crystal growth during the cooling process through the mathematical description and numerical simulation of the modified phase-field theory. Traditional ways of modeling crystallization in polymers are based on the work of Avrami.[11–13] The Avrami equation has been used widely in modeling quiescent crystallization, and variations of the Avrami equation have been proposed to account for nonisothermal conditions. Cooling from the melt can be thought of as passing through a succession of isotherms, each at a given crystallinity level, the rate of growth going through a maximum as the temperature of crystallization is lowered. However, it is a phenomenological theory that does not have a strong thermodynamic basis. Another more tested theory in polymer crystallization is the Lauritzen–Hoffman (LH) nucleation theory, which describes the deposition of a chain segment on a flat substrate and the subsequent attachment of additional stems on adjacent sites. The polymer chains form primary nuclei by overcoming the free energy barrier to crystallization with a thermal driving force, which is followed by an increase in the lamellar thickness and therefore a reduction in the free energy. As kinetic theories, the original Avrami equation and LH theory consider only the temporal development and lack spatial diffusion of the interface; hence, they are not capable of predicting the spatiotemporal crystal growth or the evolution of the shape of the crystal. Most simulations use the classical Frank model,[14] in which the moving crystallization front is treated to have an interface of zero thickness. State variables are computed in either phase separately with an independent evaluation of the interface. Such a moving boundary problem often leads to mathematical complications and is not realistic for polymer crystallization because the polymer crystal–amorphous interface is diffuse. To circumvent this problem, it is advantageous to employ front propagation with a crystal–melt interface of nonzero thickness, such as the propagation of an interface in the form of a solitary wave.

An alternative to describing polymer melt solidification is the phase-field model, in which the melt–

crystal front is treated as a spatially diffuse interface of finite thickness through the expression of order parameters.[15–19] It consists of a coupled pair of parabolic, nonlinear, partial differential equations including a heat equation. The advantage of the phase-field model over other diffusional-growth (Laplacian) models is that there is no need for tracking the positions of the interface. This allows the whole domain to be treated in the same way numerically; the position of the interface is not tracked but is given implicitly by the level set of a scalar function of time and space. Various phase-field models have been successfully applied to the dendritic growth in small-molecule systems such as snowflakes,[17] electrochemical chemical deposition,[20,21] and metal alloys.[18] However, the extension of the phase-field model originally developed for small-molecule systems to high-molecular-weight polymers has required considerable modification as polymer molecules rarely achieve thermodynamic equilibrium during solidification because of the long-chain nature of macromolecules. To capture the semicrystalline nature of polymer crystals, the metastability of polymer crystallization has been incorporated into the phase-field model; that is, the free energy density of the solid phase must be deduced to be supercooling-dependent.[22,23]

The objective of this work was to simulate the melt solidification and crystallization phenomena in rotational molding. To capture the morphology development with crystallization behavior, a two-dimensional theoretical simulation was carried out, consisting of a phase-field model emphasizing the metastability of polymer crystallization and a heat transfer model describing the molding cycle. Molding trials were also conducted with bench-scale rotational molding equipment, and the cross sections of the molded products were examined under polarized light optical microscopy.

EXPERIMENTAL

All molding trials were conducted on a bench-scale, uniaxial rotational molding machine. The oven cavity was about 38.5 cm in length and 30 cm in inner diameter. Two electrical semicircular heating panels were responsible for heating the oven cavity, and two fans were placed in the front of the oven to ensure proper air circulation and uniform temperature distribution. Thermocouples were in position to monitor the oven temperature and the air temperature inside the mold. The measurements were recorded and analyzed with an analog–digital converter data acquisition card (6024E) and Labview 6/7 software.

The experiments were carried out with two commercial rotational molding grade linear low-density polyethylene supplied by Nova Chemicals Corp. (Calgary, Canada): NOVAPOL® TR-0535 and NOVAPOL® TR-0242. The resins will be referred to as PE5-35 and PE2-42, respectively. Molecular weight distributions were determined by high-temperature gel permeation chromatography with a Waters 150C high-temperature gel permeation chromatograph with a differential refractive-index detector in accordance with ASTM D 6474. Analytical temperature rising elution fractionation (TREF) tests were also performed with a slurry-pack technique. Specimens were dissolved in 1,2,4-trichlorobenzene (TCB) at 150°C. Crystallization was carried out from 110 to 0°C at 0.025°C/min. A slurry was obtained by the addition of acetone and Celite-545 and was then packed into a stainless steel column. Elution was carried out with TCB (2 mL/min from 24.5 to 110°C at 0.25°C/min), and the concentration of the eluted solution was monitored with an IR detector cell. The comonomer distribution broadness index was determined from TREF results and was defined as the percentage of the polymer whose composition was within 50% of the median comonomer composition,[24] low values being indicative of broader comonomer distributions. A few experiments were also carried out with a commercial injection grade polypropylene (Formolene 4100N) supplied to us by Formosa Plastics Corp. (Texas, USA). Polypropylene was considered in this work for model validation purposes because its crystallization kinetics are typically slower than those observed for polyethylene. The molecular characteristics and key material properties of all resins considered in this work are presented in Table I, all data being provided by the suppliers unless noted otherwise.

All resins were received in a powder form and molded to generate parts with an average thickness of 5 mm with an aluminum box mold [$8 \times 8 \times 15$ cm^3 (inner cavity)]. The mold rotation speed was set to 6 rpm, and the oven temperature was kept constant throughout the heating cycle (270°C). The heating time varied, depending on the oven temperature required to achieve an inside air temperature of 190 $\pm$ 2°C. The air temperature inside the mold was monitored and used to control the molding cycle. Correlations between the peak internal air temperature and the mechanical properties of the molded part have been established.[25] Over the years, it has become standard procedure to use the air temperature inside the mold as an indicator in the determination of the time required for the completion of the heating cycle (melt densification) before the occurrence of polymer degradation upon exposure to high temperatures. During the cooling stage of the molding process, the mold remained in rotation while being subjected to two different cooling conditions: still air and water spray (single water spray).

Qualitative information about the crystalline structure was obtained from microphotographs of the

TABLE I
Material Properties

Resin	Type	Melt flow index (g/10 min)[a]	Density (g/cm^3)[a]	M_w (g/mol)[d]	M_w/M_n[e]	CDBI[f]
PE5-35	Ethylene–hexene copolymer	5.0[b]	0.935	69,300	3.55	29.1
PE4-42	Ethylene–hexene copolymer	1.8[b]	0.942	90,600	3.47	50.7
PP4100	Polypropylene homopolymer	20.0[c]	0.906	—	—	—

[a] Provided by the material's supplier.
[b] At 190°C (ASTM D 1238).
[c] At 230°C (ASTM D 1238).
[d] Weight-average molecular weight.
[e] Weight-average molecular weight/number-average molecular weight.
[f] Comonomer distribution broadness index.

cross sections of the molded parts. Thin layers along the cross sections (20 μm) of the parts were cut with a Leica RM2165 microtome. The specimens were viewed under an Olympus BX60 polarized light optical microscope, and pictures were taken in areas close to each edge (mold and free surfaces) with appropriate magnification.

The melting and crystallization of the polymer were studied through differential scanning calorimetry (DSC) and hot-stage microscopy techniques (Mettler FP82hot-stage unit and Olympus BX60 optical microscope coupled with a CCD monochrome camera). Variations in the equilibrium melting temperature (T_m^0) with changes in the molecular structure were taken into consideration in this work. Although T_m^0 is commonly taken to be 144.5°C for a linear polyethylene having an infinite molecular weight, this value is known to decrease with an increasing degree of branching. T_m^0 was determined experimentally from isothermal crystallization tests conducted with a TA Instruments Q100 differential scanning calorimeter. The specimens weighed in the range of 4–6 mg, and during the DSC measurements, dried N_2 gas was purged at a constant flow rate. The specimens were first heated to 200°C at 10°C/min and maintained at that temperature for 10 min. The specimens were then cooled at a rate of 10°C/min to 0°C for a nonisothermal crystallization behavior study. For isothermal crystallization experiments, the specimens were quenched from the melt to the predetermined crystallization temperature at a rate of 100°C/min and held at that temperature until the crystallization was completed. Thereafter, the specimens were heated again to obtain the DSC endotherms at a rate of 10°C/min. T_m^0 of the resins was obtained through a Hoffman–Weeks plot.[26] For the measurement of the spherulite growth rate, the aforementioned hot-stage microcopy unit was used. To ensure better temperature control and avoid thermal oxidation, the hot stage was cooled with nitrogen gas. The specimens (20 μm thick) were prepared with a Leica RM2165 microtome. The films were heated between a glass slide and a cover slip in the hot stage to 200°C for 30 min before rapid cooling to the isothermal crystallization temperature.

THEORETICAL MODELING

Heat transfer model

The thermal analysis of the process is usually limited to the consideration of two modes of energy transfer, conduction and convection.[6–9] The energy is conducted through the mold wall to the polymer powder as it melts, densifies, cools, and crystallizes against the mold wall. The heated air in the oven convects its energy through contact with the outer surface of the mold, and the air inside the mold cavity is heated and cooled through convection by the inner polymer surface.

For heat conduction through the polymer material, the energy equation can be expressed in one-dimensional Cartesian geometry as[8]

$$\frac{\partial}{\partial z}\left(k\frac{\partial T}{\partial z}\right) = \frac{d}{dt}(\rho C_p T) + q \tag{1}$$

where k is the thermal conductivity of the polymer, ρ is the density of the polymer system, and C_p is the specific heat capacity. The q term takes into account the latent heat of transition of the material, which takes positive values during melting and negative values during crystallization. Usually, the enthalpy associated with a phase transition is expressed as a function of the degree of melting (X_m) and the degree of crystallization (X_c).[8] In this way, the energy equation becomes

$$\frac{\partial}{\partial z}\left(k\frac{\partial T}{\partial z}\right) = \frac{d}{dt}(\rho C_p T) + \rho H_m \frac{dX_m}{dt} \text{ when heating} \tag{2}$$

$$\frac{\partial}{\partial z}\left(k\frac{\partial T}{\partial z}\right) = \frac{d}{dt}(\rho C_p T) - \rho H_c \frac{dX_c}{dt} \text{ when cooling} \tag{3}$$

where H_m and H_c are the total latent heats related to the melting and crystallization phase transitions and the degree of transition is defined as the ratio between the mass that has already undergone the transition at time t and the total mass. The values for these parameters were obtained through DSC measurements.

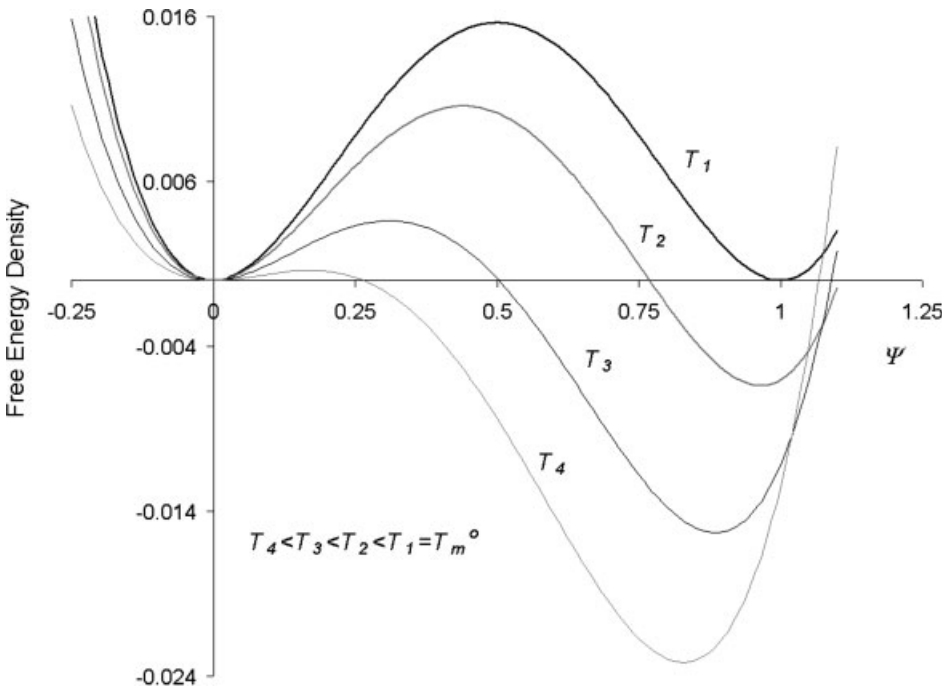

Figure 2 Variation of the local free energy density as a function of crystal order parameter ψ for various temperatures showing different nucleation barrier heights and locations (ζ). The crystal state $\psi = \psi_0$ varies with the crystallization temperature, indicating the imperfection of the polymer crystals.

The boundary conditions at the interface of the different regions are characterized by different material properties. The heat exchange at the outside surface (OS) of the mold is governed by convection:

$$-k_s \left.\frac{\partial T}{\partial z}\right|_{os} = h_o(T_o - T_{os}) \tag{4}$$

where k_s is the thermal conductivity of mold and T_o is the oven temperature. h_o and T_{os} represent the convective coefficient and the mold temperature at the oven-mold interface. At the mold–polymer interface, because of the large change in thermal transfer properties across this interface, there will be a change in temperature as the polymer lags the mold temperature; the boundary condition can be written as

$$-k_s \left.\frac{\partial T}{\partial z}\right|_{sp} = -k_p \left.\frac{\partial T}{\partial z}\right|_{ps} \tag{5}$$

where subscripts s and p indicate the mold and polymer, respectively.

At the polymer–air interface (the inner surface of the molded part), the heat exchange is assumed to be convection-controlled:

$$h_a(T_{pa} - T_a) = -k_p \left.\frac{\partial T}{\partial z}\right|_{pa} \tag{6}$$

where h_a and T_{pa} represent the convective coefficient and the temperature of the polymer at the polymer-air interface, and T_o is the internal air temperature. The initial condition is the mold, polymer, and air being at room temperature (25°C).

Phase-field model

A phase-field model that considers the metastability of polymer crystallization is used to describe the development of the spatiotemporal morphology during the cooling process in rotational molding. In phase-field modeling, the Ginzburg–Landau free energy[15–19] is constructed for a pure material to treat the system as a whole. The total free energy of the nonconserved crystal ordering $[F(\psi)]$ involves a local free energy density $[f_{\text{local}}(\psi)]$ and a nonlocal gradient term $[f_{\text{grad}}(\psi)]$, which represent nucleation and growth separately:

$$F(\psi) = \int f_{\text{cryst}}(\psi) d\Omega = \int [f_{\text{local}}(\psi) + f_{\text{grad}}(\psi)] d\Omega \tag{7}$$

It is assumed to evolve as

$$\frac{\partial \psi(r,t)}{\partial t} = -\Gamma \frac{\delta F(\psi)}{\delta \psi(r,t)} \tag{8}$$

where $\psi(r,t)$ represents the crystal order parameter at time t and position r, Ω is the integration field, and Γ is the mobility. Equation (8) is known as the time-dependent Ginzburg–Landau theory or model A equation.[19]

The crystal T_m value obtained at a given crystallization condition is always different from T_m^0. It is therefore customary to consider various metastable solid states in polymer solidifications, which reveal various hierarchy

TABLE II
Numerical Values for the Parameters of PE5-35 Used in the Models

Parameter	Value	Parameter	Value
k_s (W/m K)[a]	147	C_{pa} (J/kg K)[b]	1010
$k_{p\infty}$ (W/m K)[b]	0.2	σ (J/m^2)[c]	0.0137
ρ_s (kg/m^3)[a]	2800	v (m/s at 118°C)	1.03×10^{-7}
ρ_{powder} (kg/m^3)[b]	350	H_c (kJ/kg)	143.4
ρ_m (kg/m^3)[b]	900	H_m (kJ/kg)	140.8
ρ_c (kg/m^3)	935	h_0 (W/m^2 K)	12
ρ_a (kg/m^3)[b]	0.95	h_a (W/m^2 K)[b]	5
C_{ps} (J/kg K)[a]	917	T_m^0 (°C)	128.14

[a] Taken from ref. 6.
[b] Taken from ref. 8.
[c] Taken from ref. 40.

morphologies such as disordered spherulites and highly ordered single crystals. To account for the metastability and defective polymer crystals, the local free energy density of the system [$f_{local}(\psi,T)$] is assumed to be a monotonic function of temperature $T(r,t)$ and has the form of an asymmetric double well with respect to ψ:

$$f_{local}(\psi, T) = W \int_0^{\psi} \psi(\psi - \zeta)(\psi - \psi_0) d\psi = W\left[\frac{\zeta\psi_0}{2}\psi^2 - \frac{\zeta + \psi_0}{3}\psi^3 + \frac{\psi^4}{4}\right] \quad (9)$$

where ζ represents the value of order parameter ψ at the nucleation barrier peak and W is a dimensionless coefficient describing the height of the energy barrier for nucleation. Both ζ and W are related to the supercooling. The term ψ_0 is defined as the ratio of T_m to T_m^0. ψ_0 is proposed to describe the free energy minimum representing the metastable solid crystal, that is a function of supercooling according to the Hoffman–Weeks relationship.[26] As shown in Figure 2, the stable solid can be varied from some finite values of ψ_0 to unity at equilibrium, thereby capturing various metastable states. At T_m^0 ($\zeta = 0.5$), the free energy density has an identical local minimum, which means that the crystal and melt can coexist. When T is less than T_m^0 ($\zeta < 0.5$), the free energy density has a global minimum at $\psi_0 < 1$, representing the semicrystalline nature. In this case, the solid state is nonetheless more stable than the melt. Hence, the melt will solidify by overcoming the nucleation barrier peak labeled by ζ on the ψ axis. As the supercooling increases, ψ_0 shifts to the left to become lower than 1, and this means that the final obtained crystal contains more defects.[22,23] The uniqueness of the proposed approach is that there is no need for considering multiple metastable wells to account for the metastability potentials of polymer crystallization; a simple free energy double well with various (supercooling-dependent) ψ_0 values would serve the same purpose

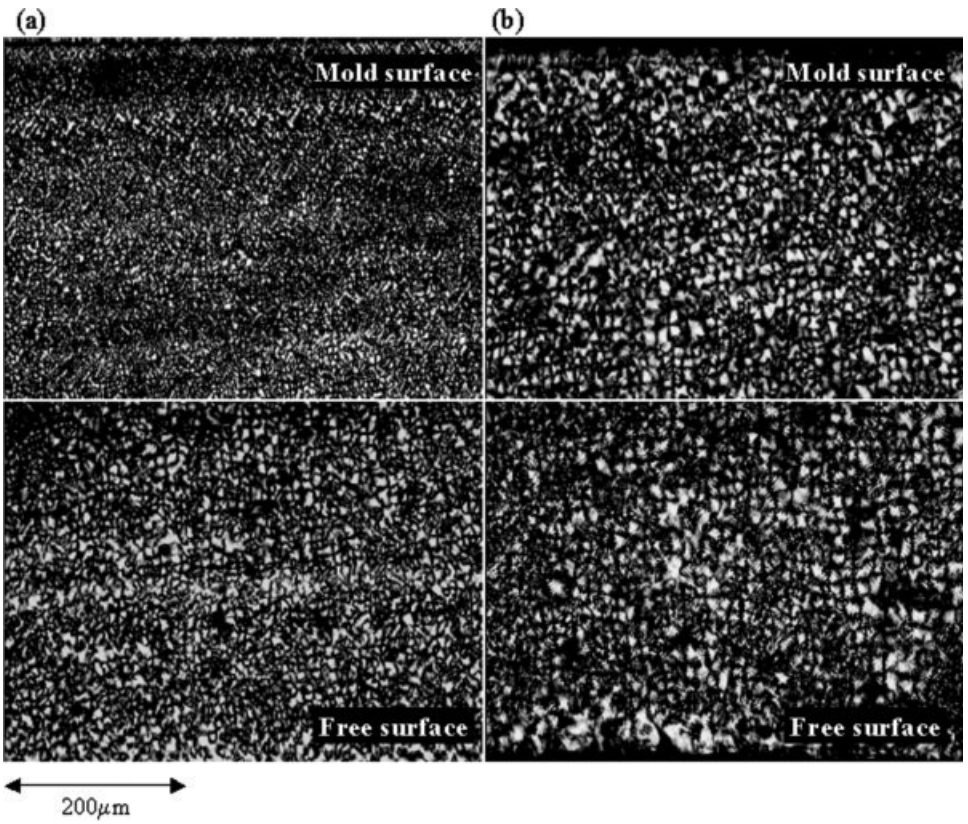

Figure 3 Polarized light microphotographs of the molded part cross section for PE5-35 processed with (a) water-spray and (b) still-air cooling conditions.

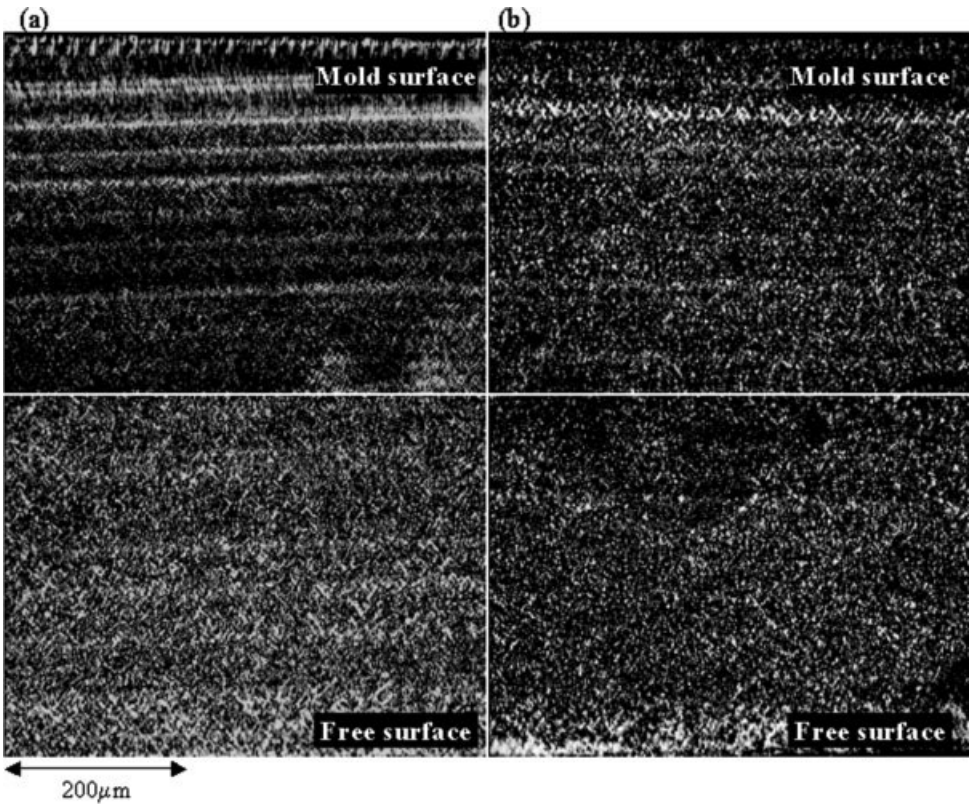

Figure 4 Polarized light microphotographs of the molded part cross section for PE2-42 processed with (a) water-spray and (b) still-air cooling conditions.

without losing the physical essence of the general solidification.

The non-local free energy density can be written in terms of the gradient free energy density [$f_{\text{grad}}(\psi)$], describing the growth process as follows:

$$f_{\text{grad}}(\psi) = \frac{1}{2}(\kappa \cdot \nabla\psi)^2 \tag{10}$$

where κ is the gradient coefficient depending on the crystal–melt interface property. Substituting eqs. (9) and (10) into eq. (8), one obtains

$$\frac{\partial\psi(r,t)}{\partial t} = -\Gamma\frac{\delta F(\psi)}{\delta\psi} = -\Gamma\left[W\psi(\psi-\zeta)(\psi-\psi_0) - \kappa^2\nabla^2\psi\right] + \eta_\psi \tag{11}$$

where η_ψ is the uncorrelated Langevin noise term. It is well known that the temperature plays a significant role in the crystallization process. The temperature distribution inside the bulk during the cooling stage can be determined with the modified heat transfer equation:

$$\frac{\partial}{\partial z}\left(k\frac{\partial T}{\partial z}\right) = \frac{d}{dt}(\rho C_p T) - \rho H_c X_c \frac{d\psi}{dt} \tag{12}$$

When crystallization starts, the melt–solid transition happens at the crystal growth front, and the second term on the right side takes account of the liberation of latent heat.

During rotational molding, the density of nuclei is greatly affected by the cooling conditions, increasing at a lower temperature or a faster cooling rate. The nucleation process is simulated with the introduction of η_ψ into the crystallization equation [eq. (11)] with amplitudes that are determined by the fluctuation–dissipation theorem.[27,28] With cooling from the outer surface toward the inner wall, some noises are activated by the nucleation energy barrier being overcome, which is determined by the supercooling. As demonstrated by Allen and coworkers[29,30] and Wheeler et al.,[31] in the phase-field model, the parameters can be evaluated on the basis of the material (or physical) properties, which can be determined experimentally (see the appendix).

NUMERICAL MODEL

During the simulation, the numerical values of the parameters were obtained from the experimental results. The heat-transfer coefficients for the oven were assessed by temperature measurements made on empty molds rotating in the oven. The data-logger-

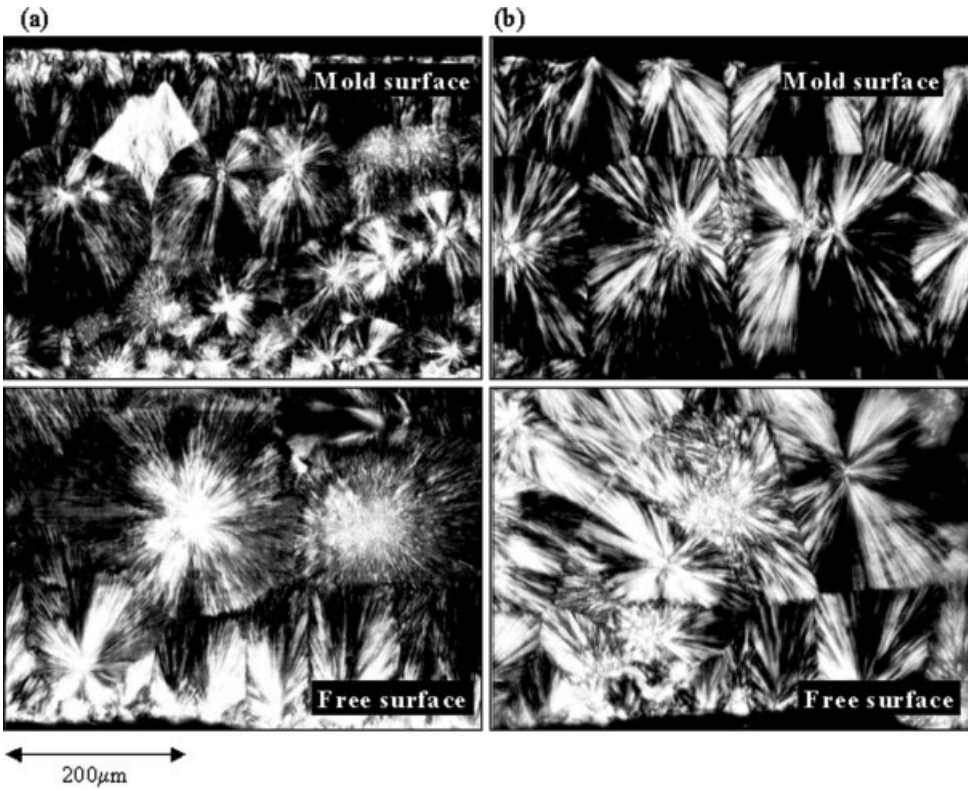

Figure 5 Polarized light microphotographs of the molded part cross section for PP4100 processed with (a) water-spray and (b) still-air cooling conditions.

recorded temperature profile was compared with the simulated outputs for various heat-transfer-coefficient values until the predicted curve matched the experimental measurement. For the polymer resin, the variations of the physical and thermal properties with the temperature had to be considered. The temperature dependence of the heat capacity was obtained from DSC measurements of the polymer. The density (ρ) was considered to be a function of X_m during heating and X_c during cooling with a simple linear mixing rule for simplicity:

$$\rho = X_m \rho_m + (1 - X_m)\rho_{\text{powder}} \quad \text{(heating)} \tag{13}$$

$$\rho = X_c \rho_c + (1 - X_c)\rho_m \quad \text{(cooling)} \tag{14}$$

where ρ_{powder} is the bulk density of the powder, ρ_c is the density of the crystal, and ρ_m is the density of the melt. Similarly, the thermal conductivity of the polymer was evaluated by means of the mixing rule, as the thermal conductivity of a polymer system is a function of density:

$$k_p = \frac{\rho}{\rho_c} k_{p\infty} \tag{15}$$

with $k_{p\infty}$ being the thermal conductivity of the polymer crystal. No variation of the thermal properties was assumed for the mold material.

With the isothermal crystallization in DSC and hot-stage microscopy, T_m^0 was measured by the Hoffman–Weeks method.[26,32,33] The interfacial growth velocity (v) was examined through optical microscopy by an examination of the spherulite radius growth as the crystallization time proceeded. The surface energy (σ) was evaluated according to Lauritzen and Hoffman's calculation.[34] In the phase-field simulation, all of the model parameters were temperature-dependent. Additionally, as described in the appendix, the height of the energy barrier to nucleation (W) was determined with H_c and T_m^0. κ was evaluated from σ, and Γ was calculated with both v and σ. The heat of crystallization and equilibrium temperature were determined from DSC measurements, whereas the growth velocity was obtained from isothermal crystallization tests conducted with a hot-stage microscope and image analysis unit.

The proposed equations were solved numerically using the central finite difference method for spatial discretization and the explicit forward difference method for time steps. Two-dimensional calculations were undertaken to evaluate the heating cycle during the rotational-molding process. In the two-dimensional simulations, various grid sizes (128×128, 256×256, and 512×512) and temporal steps (Δt) were employed to ascertain the stability of the simulation; however, only the results of the 512×512 simula-

tion are presented. The numerical values of the parameters are listed in Table II, where p_a and C_{p_a} represent the density and heat capacity of air, while p_s and C_{ps} represent those of the mold.

RESULTS AND DISCUSSION

Experimental results

The micrographs obtained with polarized light microscopy revealed that the general crystalline texture of the samples was mainly spherulites with well-defined Maltese crosses and regularly spaced dark bands; these are typical features of polyethylene. Figures 3–5 show the cross-sectional morphologies obtained for all resins under different cooling conditions. Characteristic cooling rates were estimated from the profiles of the air temperature inside the mold, as shown in Figure 6. A close examination of the experimental data presented in the literature[7,4] shows that, for the cooling and melt solidification stages of the process, the profile of the air temperature inside the mold provides a very good estimate of that measured within the polymer layer, though showing a time shift, as expected from the thermal analysis of the process. It is apparent that the cooling rate has a significant impact on the resulting microstructures. Morphology changes with cooling conditions, however, are not as important for PE2-42 as for PE5-35 and PP4100. The nucleation density for PE2-42 would be expected to be higher than that for resins with higher comonomer contents (i.e., higher branching contents and lower densities). All the ethylene copolymers were produced with a gas-phase Ziegler–Natta catalyst system, which resulted in the production of molecules with nonuniformly distributed comonomers among and within molecules and thus a nonuniform branching distribution. An increase in the degree of branching reduced the surface nucleation rate more than the lateral spreading rate.[35] All the ethylene copolymers showed a coarsening and deterioration in the spherulitic structure with a decreasing cooling rate. Under air cooling conditions, crystallization occurs at higher temperatures, which are associated with lower nucleation rates. Lower cooling rates provide sufficient time for polymer long chains to arrange themselves into ordered structures during crystallization, resulting in spherulite structures that evolve into stacked lamellae. Our observations are consistent with those presented in the literature with narrow fractions of ethylene copolymers.[36]

Variations in the morphological features across the thickness of the molded part are generally expected for rotationally molded products. Cramez et al.[3] showed that the size of the spherulites increases from the mold surface toward the free surface with rotational-molded polypropylene of 12-mm thickness. Our experimental results showed the same tendency, and the difference in the spherulite size is recognizable with a smaller thickness. Because of the higher thermal conductivity of the metal mold, the regions in close contact with the mold wall cool at a faster rate, leading to a sharper temperature gradient than that of the inner surface zone. However, along the surface contacting the mold wall, all samples displayed a transcrystalline layer. A large number of heterogeneous nuclei are activated at the polymer–

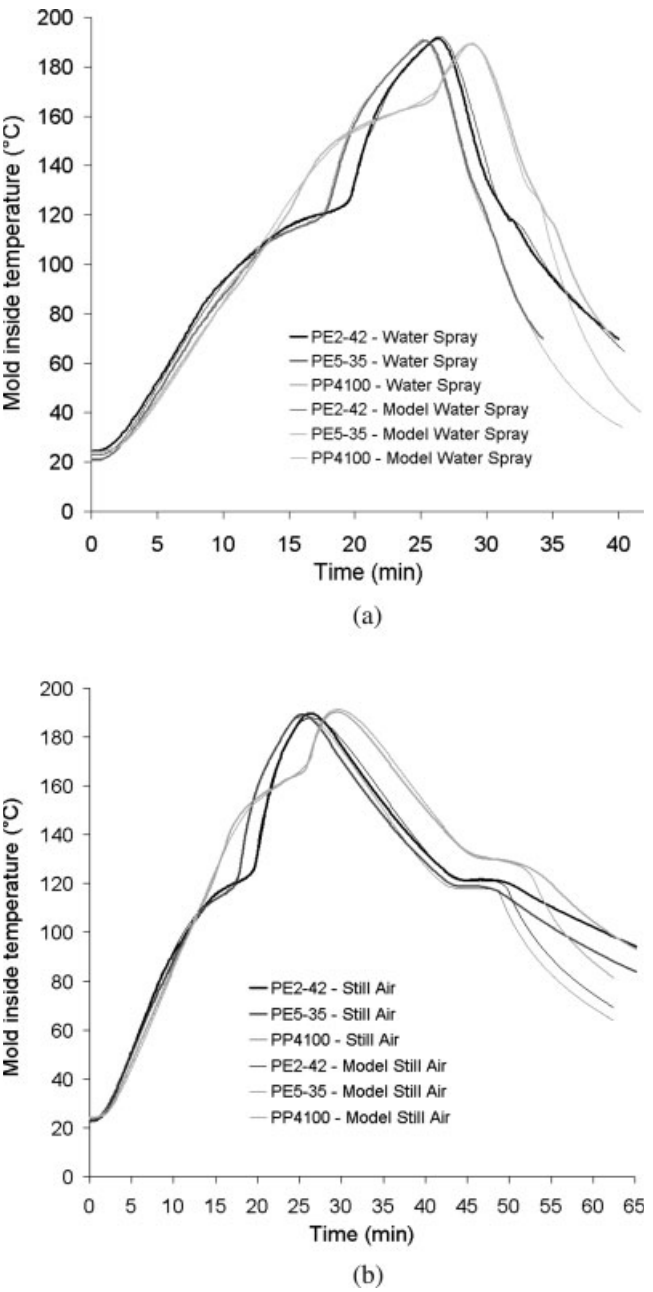

Figure 6 Temperature profiles for PE5-35, PE2-42, and PP4100 when processed with (a) water-spray and (b) still-air cooling conditions.

TABLE III
Melting Temperature (T_m) and Heat of Fusion (ΔH_f), Determined by DSC, of Specimens Taken from Molded Parts

	Air cooling conditions		Water-spray cooling conditions	
Resin	T_m (°C)	ΔH_f (J/kg × 10^3)	T_m (°C)	ΔH_f (J/kg × 10^3)
PE5-35 (mold surface)	126.4	143.2	126.6	124.9
PE5-35 (free surface)	127.6	135.7	127.5	122.5
PE4-42 (mold surface)	130.8	154.1	127.9	157.6
PE4-42 (free surface)	130.2	163.6	128.7	161.8
PP4100 (mold surface)	164.5	81.8	165.5	82.4
PP4100 (free surface)	161.6	98.2	160.8	97.8

mold interface, and they tend to grow parallel to the temperature gradient direction. In the absence of degradation, the free growth of spherulites leads to a great roughness at the inner surface. Variations in the morphological features across the thickness of the molded part were more apparent for parts produced under severe cooling conditions (water spray) and with low-density polyethylene resins as well as polypropylene.

The stability of the crystalline structure across the thickness of the molded part was evaluated with DSC, and the results are summarized in Table III. Crystalline structures with lower stability crystallize and melt at lower temperatures. Although crystalline structures generated under slow cooling conditions tend to show a higher degree of stability and perfection (Table III), they are expected to show a lower failure strain because an increase in the size of the spherulitic structure is often accompanied by a reduction in the interspherulitic boundary links. This in turns allows for the easier transmission of energy through the material and thus causes a loss in the ductility. This problem can be alleviated with faster cooling rates, which, on the other hand, lead to the generation of higher residual stresses in the parts, which would explain the increased warpage observed for all molded parts produced under such conditions. Rapid cooling can be achieved by use of forced convection and exposure of the mold to the spray of water. Such conditions produce parts with a lower degree of crystallinity (Table III) and give rise to smaller spherulitic structures (Figs. 3–5).

Model predictions

The model predictions for the temperature profile were validated against data collected during the molding experiments. Figure 6 shows the simulated internal air temperature profiles under different cooling conditions with heat-transfer modeling. A good agreement was obtained with the experimental measurements in light of the variation of the operation environments. With an increase in the cooling severity, the cycle time was reduced, and the crystallization region became narrower with a faster cooling rate. For the still-air cooling condition, there appeared a deviation between the experimental measurements and modeling results immediately after the crystallization was completed. This might have been caused by the separation of the polymer part from the mold surface. Because of the crystallization and the formation of thermally induced residual stress inside the polymer part, the molded part tended to shrink itself, and this introduced an air gap between the part and mold surface. Thus, it reduced the cooling effect and let the polymer part stay for a longer time at a high temperature.

The experimentally observed morphology has been simulated with the two-dimensional phase-field model with the calculated temperature distribution, Figure 7 shows the spatiotemporal spherulite growth under the

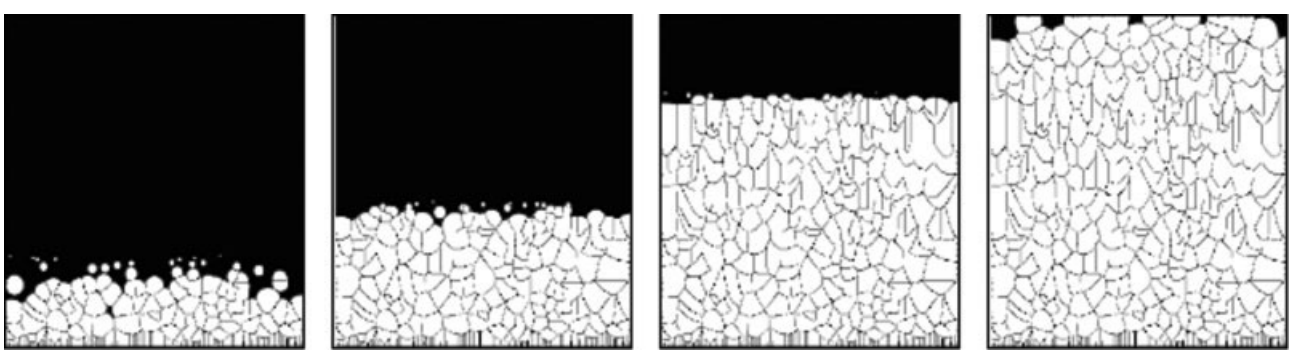

Figure 7 Simulation results showing the spatiotemporal morphology under water-spray cooling conditions.

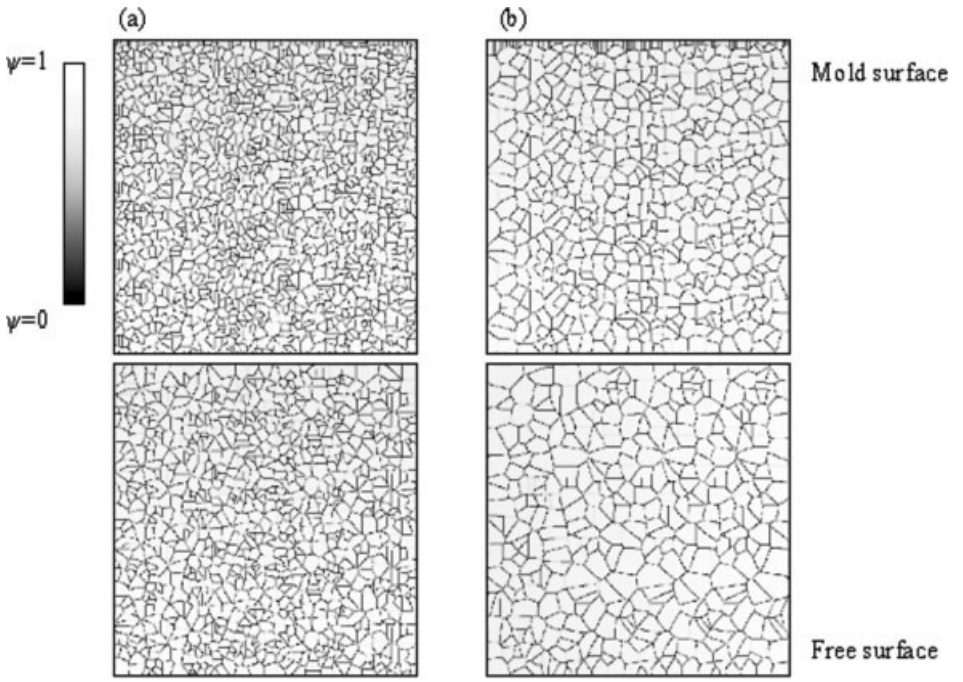

Figure 8 Simulation results showing the morphology of a 5-mm-thick cross section of PE5-35 processed with (a) water-spray and (b) still-air cooling conditions.

water-spray cooling condition. As the cooling proceeded, the mold surface zone cooled first, and a large number of nuclei appeared along the polymer–mold interface. Because of the geometric restriction, these nuclei were closely distributed and could grow only inward; this transferred the sphere growth to a one-dimensional, transcrystalline texture. As cooling continued, some cold noises gained higher amplitudes and were able to overcome the critical nucleation energy barrier. The material cooled from the outer surface

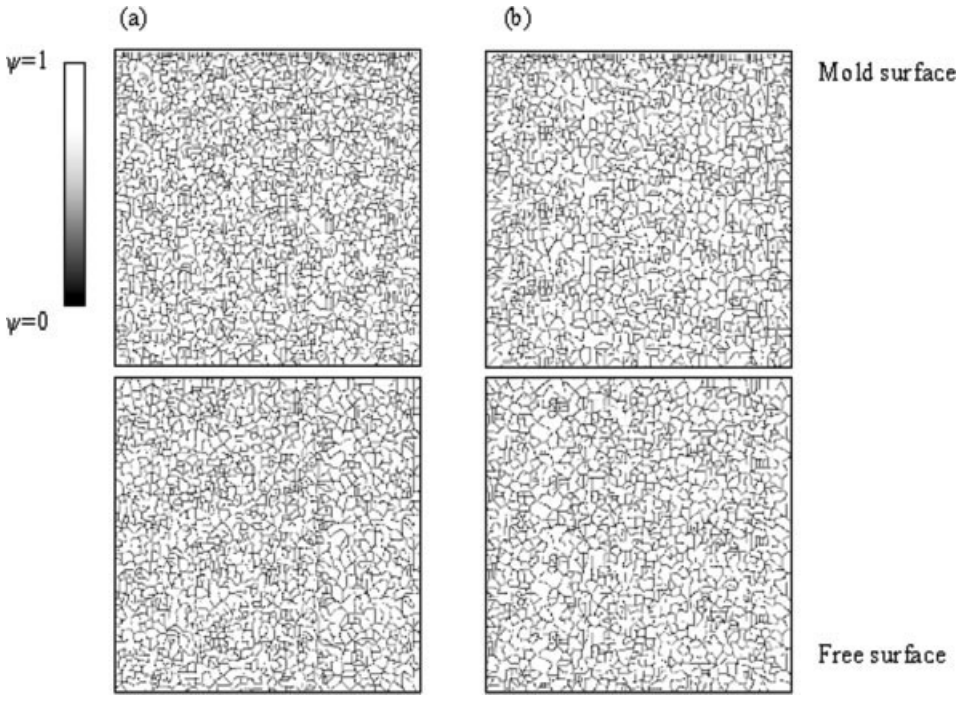

Figure 9 Simulation results showing the morphology of a 5-mm-thick cross section of PE2-42 processed with (a) water-spray and (b) still-air cooling conditions.

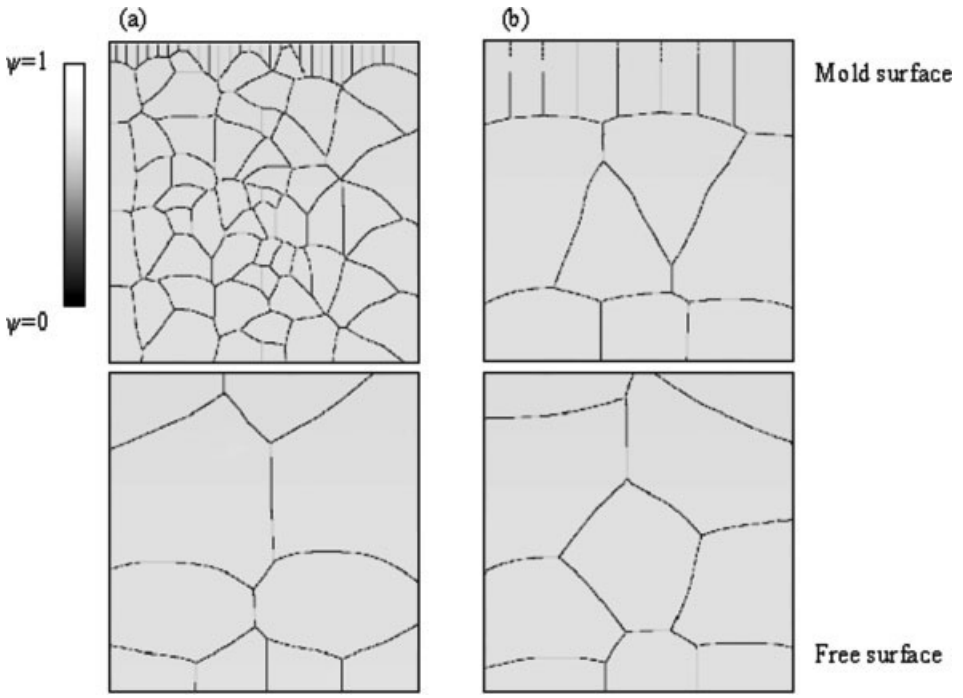

Figure 10 Simulation results showing the morphology of a 5-mm-thick cross section of PP4100 processed with (a) water-spray and (b) still-air cooling conditions.

(bottom) toward the inner surface (top), and more nuclei formed and grew into spherulites. Individual spherulites continued growing until they reached neighboring spherulites. When the impingement happened, the grain boundary formed because of the misorientation between different spherulites,[37] resulting in polyhedral shapes. Because of the vertical cooling direction, some spherulites were elongated, tending to grow parallel to the temperature gradient direction; a phenomenon which has already been reported by Lovering.[38]

The simulation results for the three resins molded under different cooling conditions are reported in Figures 8–13. We report only morphological features as predicted at the end of the cooling stage. The results demonstrate the effect that cooling conditions have on the nature of the spherulitic growth and the subsequent morphology. With the water-spray cooling method, the crystallization time at higher temperatures is shortened, favoring a higher nucleation rate and inhibiting the diffusion of polymer chain move-

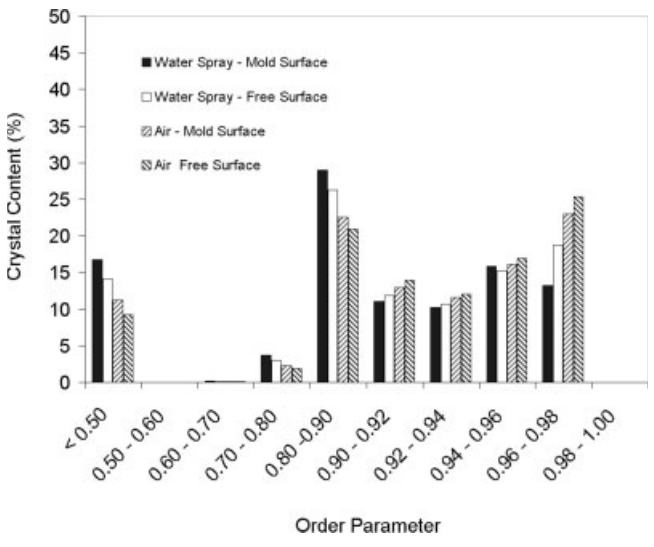

Figure 11 Order parameter distribution profile for PE5-35.

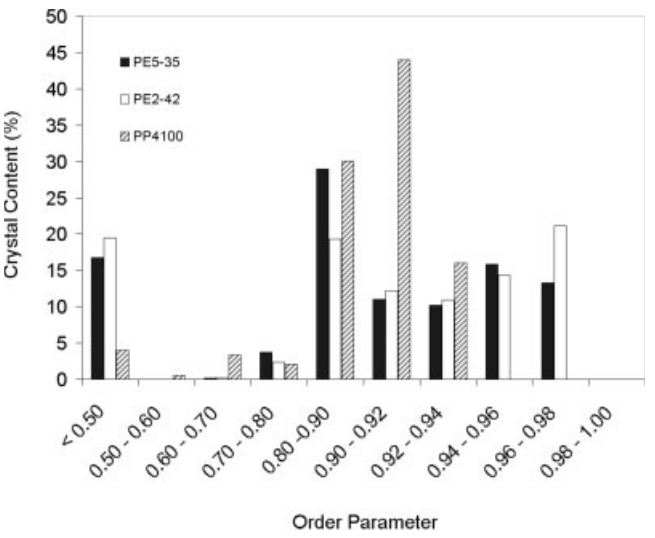

Figure 12 Order parameter distribution profile obtained near the mold surface with water-spray cooling conditions for PE5-35, PE2-42, and PP4100.

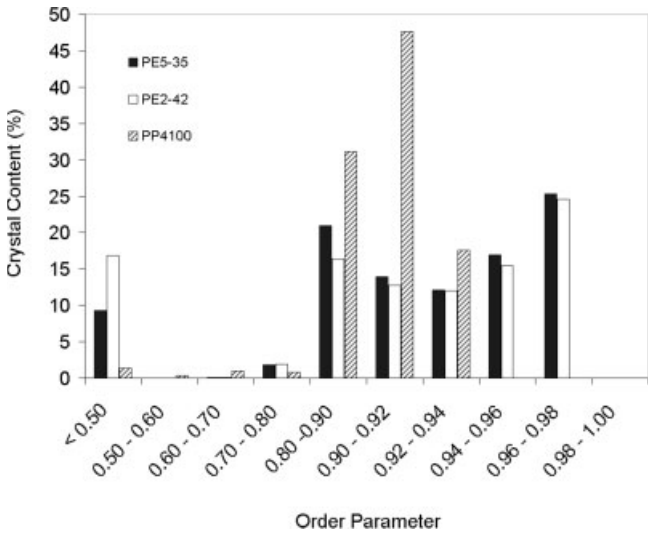

Figure 13 Order parameter distribution profile obtained near the free surface with still-air cooling conditions for PE5-35, PE2-42, and PP4100.

ment. The simulated picture displays finer spherulitic structures. At a lower cooling rate (still-air cooling), diffusion is facilitated, and multiple nucleations are inhibited; this leads to more perfect lamellae and hence higher crystallinity. The phase-field model predictions for the metastable crystal states can provide information about the various hierarchy morphologies, such as disordered spherulites and highly ordered crystals. The metastable crystal ordering (ψ_0) is proposed to be crystallization-temperature-dependent, capturing various metastable states from some finite values (less perfect crystal) to unity (perfect crystal) at equilibrium. In the ψ_0 distribution plot of PE5-35 (Fig. 11), we can see that under the still-air cooling condition, more ordered crystals with a higher value of ψ_0 were obtained than under the water-spray cooling conditions, which means that it produced more stable crystals and more perfect lamellae inside the spherulites. When the ψ_0 value dropped to 0.8–0.9, the crystallization temperature was already much lower, which occurred in a late cooling stage when many imperfect crystallites were formed. At $\psi_0 < 0.5$, the material was considered to be in an amorphous state, including the defective spherulite boundary. In this way, the spherulite size is related directly to the captured crystal metastability. Additionally, because the mold surface zone cooled at a faster rate and earlier in the process, it produced a sharper temperature gradient. As a result, more nuclei were triggered, producing smaller crystallites. At the polymer–mold interface, the small spherulites gave way to a transcrystalline layer consisting of bundles of parallel fibrils. In addition, the simulations captured less ordered crystals at the mold surface zone than at the free surface. Under the still-air cooling condition, this kind of fibril grew much longer inward until it collided with the internal spherulites (Figs. 8–10). The simulation showed the same effect of the cooling conditions as the experiments.

The results reported in Figure 11 are consistent with those reported in Table III. Figures 12 and 13 present a comparison of the prediction results among the three resins considered in this work. The most stable crystalline structures when rotational molding grade polyethylene was processed appeared near the free surface under slow cooling conditions. The reduction in the degree of crystallinity and/or T_m in the region near the free surface compared with the mold surface (Table III) suggested that changes in the molecular structures took place because of thermooxidative degradation reactions. The kinetics of the degradation reactions would need to be taken into consideration to capture all features of the rotational-molding process. Despite this omission in the model proposed in this article, the predictions reported in Figures 8–13 are overall in very good agreement with the experimental observations reported for the polypropylene resin and polyethylene copolymers.

CONCLUSIONS

According to the experimental and modeling work for the rotational-molding process, semicrystalline polyethylene undergoing the entire heat cycle displays a spherulite morphology with a structure gradient under asymmetrical cooling conditions. Accounting for the metastability of polymer crystallization, the modified phase-field model successfully captures the spatiotemporal morphology development in the rotational-molding process by coupling the nonconserved crystal order parameter and the temperature field. In the two-dimensional simulation, the nucleation and crystal growth are proposed to be temperature-dependent. Both the experimental observations and simulation results show that the cooling rate has an important effect on the morphology of the materials. Under severe cooling conditions, finer spherulite structures have been observed, and the average density of the nuclei increases with an increase in the cooling rate. The transcrystalline structure at the polymer interfaces has also been captured theoretically. The model has been used to evaluate the degree of stability of the morphological structure across the molded part. Our results show that the model predictions successfully capture variations in the morphological features caused by changes in the material formulation as well as changes in the molding conditions. This modeling approach should enable significant advances in the development of the relationship between the material formulation, processing conditions, and properties of rotationally molded products.

APPENDIX: DETERMINATION OF THE MODEL PARAMETERS IN THE PHASE-FIELD MODEL

At a given crystallization temperature T, a crystal of stable lamellar thickness l_z is formed with a change in the local free energy (Δf_{local}):

$$\Delta f_{\text{local}} = 2A\sigma_e - Al_zH_c(1 - T/T_m^0) \tag{A.1}$$

where σ_e is the surface free energy per unit of area of folded surface A. The crystal order parameter can be defined as $\psi = l/l_z$. In Figure 2, we find that at $\Delta f_{\text{local}} = 0$, there exists a lamellar thickness $l^* < l_z$ at the stability order parameter $\psi^* = l^*/l_z$, so

$$2\frac{\sigma_e}{l^*} - H_c(1 - T/T_m^0) = 0 \tag{A.2}$$

According to the Hoffman–Weeks relationship,[26] T_m of the crystal prepared at a given crystallization temperature T can be related to lamellar thickness l_z:

$$2\frac{\sigma_e}{l_z} - H_c(1 - T_m/T_m^0) = 0 \tag{A.3}$$

Then, ψ^* can be obtained from eqs. (A.2) and (A.3):

$$\psi^* = \frac{l^*}{l_z} = \frac{T_m^0 - T_m}{T_m^0 - T} \tag{A.4}$$

When inserted into eq. (9), the maximum position in the free energy of crystallization (ζ) is related to the supercooling as

$$\zeta = \frac{4\psi_0\psi^* - 3\psi^{*2}}{6\psi_0 - 4\psi^*} \tag{A.5}$$

On the other hand, from eq. (9), the change in the local free energy density at crystallization temperature T ($\Delta f_{\text{local}}^{\psi}$) is expressed as follows:

$$\Delta f_{local}^{\psi} = W\left(\frac{\zeta\psi_0^3}{6} - \frac{\psi_0^4}{12}\right) \tag{A.6}$$

By equating the free energy densities of crystallization given by eqs. (A1) and (A6), we obtain

$$2\frac{\sigma_e}{l_z nRT} - \frac{H_c}{nRT}(1 - T/T_m^0) = W\left(\frac{\zeta\psi_0^3}{6} - \frac{\psi_0^4}{12}\right)$$

where n is the molar density and R is the gas constant. With eq. (A3), parameter W can be written as

$$W = 6\frac{H_c}{nRT\psi_0^3}\left(\frac{T_m - T}{T_m^0}\right)\left(\frac{\psi_0}{2} - \zeta\right)^{-1} \tag{A.7}$$

According to Allen and Cahn's approach,[29,30] the excess free energy per unit of area in the interface region over the bulk phases can be given as $\sigma/nRT = \int_0^1 \sqrt{2f^{\psi}}d\psi$. At $T = T_m$, we have

$$\frac{\sigma}{nRT} = \frac{\kappa}{6}\sqrt{\frac{W}{2}} \tag{A.8}$$

Therefore

$$\kappa = 6\frac{\sigma}{nRT}\left(\frac{2}{W}\right)^{1/2} \tag{A.9}$$

If we consider eq. (11) in one dimension with a moving frame of reference under a uniform velocity of $v = \partial\psi/\partial t$, eq. (11) is transformed as

$$\kappa^2\frac{d^2\psi}{dx^2} + \frac{v}{\Gamma}\frac{d\psi}{dx} - \frac{\partial f}{\partial\psi} = 0 \tag{A.10}$$

We seek a solution of the form $\psi = \psi(z)$, where $z = x - vt$ under the boundary condition of $\psi \to \psi_0$ as $x \to -\infty$ and $\psi \to 0$ as $x \to +\infty$;[39] we have a stationary solution:

$$\psi(z) = \frac{\psi_0}{\left[1 + \exp\left(z\psi_0\sqrt{\frac{W}{2\kappa^2}}\right)\right]} \quad \text{with}$$

$$v = -\Gamma\kappa\left(\zeta - \frac{\psi_0}{2}\right)\sqrt{W} \tag{A.11}$$

Combining eqs. (A.9) and (A.11), we obtain

$$\Gamma = \frac{\sqrt{2}}{12}v\left[\frac{\sigma}{nRT}\left(\frac{\psi_0}{2} - \zeta\right)\right]^{-1} \tag{A.12}$$

All these material parameters are supercooling- or temperature-dependent, and this is exactly what one does in real experiments when probing the formation of various crystalline morphologies.

References

1. Bellehumeur, C. T.; Bisaria, M. K.; Vlachopoulos, J. Polym Eng Sci 1996, 36, 2198.
2. Kontopoulou, M.; Vlachopoulos, J. Polym Eng Sci 1999, 39, 1189.
3. Cramez, M. C.; Oliveira, M. J.; Crawford, R. J. J Mater Sci 2001, 36, 2151.
4. Martin, J. A.; Cramez, M. C.; Oliveira, M. J.; Crawford, R. J Macromol Sci Phys 2003, 42, 367.
5. Glomsaker, T.; Larsen, Å.; Andreassen, E.; Ommundsen, E. Polym Eng Sci 2005, 45, 945.
6. Rao, M. A.; Throne, J. L. Polym Eng Sci 1972, 12, 237.
7. Nugent, P. J. Ph.D. Thesis, Queen's University of Belfast, 1990.
8. Greco, A.; Maffezzoli, A.; Vlachopoulos, J. Adv Polym Technol 2003, 22, 271.
9. Gogos, G.; Olson, L. G.; Liu, X.; Pasham, V. R. Polym Eng Sci 1998, 38, 1387.
10. Lim, K. K.; Ianakiev, A. Annu Tech Conf 2004, 1, 897.

11. Avrami, M. J Chem Phys 1939, 7, 1103.
12. Avrami, M. J Chem Phys 1940, 8, 212.
13. Avrami, M. J Chem Phys 1941, 9, 177.
14. Frank, F. C. J Cryst Growth 1974, 22, 233.
15. Caginalp, G.; Fife, P. C. Phys Rev B 1986, 33, 7792.
16. Caginalp, G. Phys Rev A 1989, 39, 5887.
17. Kobayashi, R. Phys D 1993, 63, 410.
18. Wheeler, A. A.; Boettinger, W. J.; McFadden, G. B. Phys Rev A 1992, 45, 7424.
19. Kyu, T.; Mehta, R.; Chiu, H.-W. Phys Rev E 2000, 61, 4161.
20. Grier, D.; Ben-Jacob, E.; Clarke, R.; Sander, L. M. Phys Rev Lett 1986, 56, 1264.
21. Sawada, Y.; Dougherty, A.; Gollub, J. P. Phys Rev Lett 1986, 56, 1260.
22. Xu, H.; Matkar, R.; Kyu, T. Phys Rev E 2005, 72, 011804.
23. Xu, H.; Keawwattana, W.; Kyu, T. J Chem Phys 2005, 123, 124908.
24. Wild, L.; Ryle, T. R.; Knobeloch, D. C.; Peat, I. R. J Polym Sci Polym Phys Ed 1982, 20, 441.
25. Crawford, R. J.; Nugent, P. J. Plast Rubber Compd Process Appl 1992, 17, 33.
26. Hoffman, J. D.; Weeks, J. J. J Res Natl Bur Stand Sect A 1962, 66, 13.
27. Gunton, J. D.; San Miguel, M.; Sahni, P. S. In Phase Transitions and Critical Phenomena; Domb, C.; Lebowitz, J. L., Eds.; Academic: New York, 1983; p 267.
28. Zykov, V. S. Simulation of Wave Processes in Excitable Media; Manchester University Press: New York, 1987.
29. Allen, S.; Cahn, J. W. Acta Metall 1979, 27, 1085.
30. Cahn, J. W.; Hilliard, J. E. J Chem Phys 1958, 28, 258.
31. Wheeler, A. A.; Boettinger, W. J.; Mcfadden, G. B. Phys Rev A 1992, 45, 7424.
32. Hoffman, J. D.; Miller, R. L. Polymer 1997, 38, 3151.
33. Marand, H.; Hoffman, J. D. Macromolecules 1990, 23, 3682.
34. Lauritzen, J. I., Jr.; Hoffman, J. D. J Appl Phys 1973, 44, 4340.
35. Chiu, F. C.; Peng, Y.; Fu, Q. J Polym Res 2002, 9, 175.
36. Peeters, M.; Goderis, B.; Vonk, C.; Reynaers, H.; Mathot, V. J Polym Sci Part B: Polym Phys 1997, 35, 2689.
37. Kobayashi, R.; Warren, J. A.; Carter, W. C. Phys D 2000, 140, 141.
38. Lovering, E. G. J Polym Sci Part A-2: Polym Phys 1970, 8, 1697.
39. Harrowell, P. R.; Oxtoby, D. W. J Chem Phys 1987, 86, 2932.
40. Hoffman, J. D.; Davis, G. T.; Lauritzen, J. I., Jr. In Treatise on Solid State Chemistry; Hannay, N. B., Ed.; Plenum: New York, 1976; Chapter 7, p 479.